



TITLE:

Response of Jupiter's Aurora to Plasma Mass Loading Rate Monitored by the Hisaki Satellite During Volcanic Eruptions at Io

AUTHOR(S):

Kimura, T.; Hiraki, Y.; Tao, C.; Tsuchiya, F.; Delamere, P. A.; Yoshioka, K.; Murakami, G.; ... Fukazawa, K.; Yoshikawa, I.; Fujimoto, M.

CITATION:

Kimura, T. ...[et al]. Response of Jupiter's Aurora to Plasma Mass Loading Rate Monitored by the Hisaki Satellite During Volcanic Eruptions at Io. Journal of Geophysical Research: Space Physics 2018, 123(3): 1885-1599

ISSUE DATE:

2018-3

URL:

<http://hdl.handle.net/2433/242242>

RIGHT:

©2018. American Geophysical Union.; The full-text file will be made open to the public on 16 October 2018 in accordance with publisher's 'Terms and Conditions for Self-Archiving'.

RESEARCH ARTICLE

10.1002/2017JA025029

Key Points:

- Response of Jupiter's aurora to mass loading from Io was investigated with a newly developed model and data from the Hisaki satellite
- The estimated mass loading rate indicated increase and decay during volcanic eruptions at Io
- During volcanic eruptions at Io, impulsive variation of aurora responded to the mass loading rate rather than the solar wind

Correspondence to:

T. Kimura,
tomoki.kimura@riken.jp

Citation:

Kimura, T., Hiraki, Y., Tao, C., Tsuchiya, F., Delamere, P. A., Yoshioka, K., et al. (2018). Response of Jupiter's aurora to plasma mass loading rate monitored by the Hisaki satellite during volcanic eruptions at Io. *Journal of Geophysical Research: Space Physics*, 123, 1885–1899. <https://doi.org/10.1002/2017JA025029>

Received 21 NOV 2017

Accepted 20 FEB 2018

Accepted article online 27 FEB 2018

Published online 13 MAR 2018

Response of Jupiter's Aurora to Plasma Mass Loading Rate Monitored by the Hisaki Satellite During Volcanic Eruptions at Io

T. Kimura¹ , Y. Hiraki², C. Tao³ , F. Tsuchiya⁴ , P. A. Delamere⁵, K. Yoshioka⁶ , G. Murakami⁷ , A. Yamazaki⁷ , H. Kita⁴ , S. V. Badman⁸ , K. Fukazawa⁹, I. Yoshikawa⁶ , and M. Fujimoto^{7,10}

¹Nishina Center for Accelerator-Based Science, RIKEN, Wako, Saitama, Japan, ²Advanced Knowledge Laboratory, Inc., Shinjuku, Japan, ³National Institute of Information and Communications Technology, Tokyo, Japan, ⁴Planetary Plasma and Atmospheric Research Center, Tohoku University, Sendai, Japan, ⁵Geophysical Institute, University of Alaska Fairbanks, Fairbanks, AK, USA, ⁶Department of Complexity Science and Engineering, University of Tokyo, Kashiwa, Japan, ⁷Institute of Space and Astronautical Science, Japan Aerospace Exploration Agency, Sagami, Japan, ⁸Department of Physics, Lancaster University, Lancaster, UK, ⁹Academic Center for Computing and Media Studies, Kyoto University, Kyoto, Japan, ¹⁰Earth-Life Science Institute, Tokyo Institute of Technology, Tokyo, Japan

Abstract The production and transport of plasma mass are essential processes in the dynamics of planetary magnetospheres. At Jupiter, it is hypothesized that Io's volcanic plasma carried out of the plasma torus is transported radially outward in the rotating magnetosphere and is recurrently ejected as plasmoid via tail reconnection. The plasmoid ejection is likely associated with particle energization, radial plasma flow, and transient auroral emissions. However, it has not been demonstrated that plasmoid ejection is sensitive to mass loading because of the lack of simultaneous observations of both processes. We report the response of plasmoid ejection to mass loading during large volcanic eruptions at Io in 2015. Response of the transient aurora to the mass loading rate was investigated based on a combination of Hisaki satellite monitoring and a newly developed analytic model. We found that the transient aurora frequently recurred at a 2–6 day period in response to a mass loading increase from 0.3 to 0.5 t/s. In general, the recurrence of the transient aurora was not significantly correlated with the solar wind, although there was an exceptional event with a maximum emission power of ~10 TW after the solar wind shock arrival. The recurrence of plasmoid ejection requires the precondition that an amount comparable to the total mass of magnetosphere, ~1.5 Mt, is accumulated in the magnetosphere. A plasmoid mass of more than 0.1 Mt is necessary in case that the plasmoid ejection is the only process for mass release.

1. Introduction

Jupiter's rotating magnetosphere is filled with magnetized plasmas provided by the moons, rings, external solar wind, and Jupiter's atmosphere. The dominant plasma source is the moon Io. Io's volcanoes supply neutral gases, which mainly consist of mainly sulfur dioxide (SO₂) and constitutive atoms. Oxygen and sulfur atoms are created via dissociation of the neutral gases by impacts with magnetospheric ions and electrons and by photolysis. These neutral atoms escape from Io's atmosphere to the magnetosphere. Neutral gas is ionized via collisional processes with the magnetospheric electrons and is picked up by Jupiter's intrinsic magnetic field. The logenic plasma corotates with the planet, forming the Io plasma torus in the inner magnetosphere. The net rate of plasma mass transported out of the torus is estimated to be 0.26–1.4 t/s (1 t = 1,000 kg; Delamere & Bagenal, 2003; Delamere et al., 2004; Steffl et al., 2006). In the present study, we refer to this net rate as the “plasma mass loading rate” or simply “mass loading rate.” The loaded plasma circulates throughout the magnetosphere. Thermal energy, kinetic energy, and angular momentum, which are essential for magnetospheric dynamics, as well as the mass, are carried by the circulating plasma. See the reviews in Bagenal et al. (2004), Bagenal and Delamere (2011), Delamere, Bagenal, et al. (2015), Achilleos et al. (2014), Kivelson (2014), and references therein for properties of the plasma circulation.

Previous theoretical studies predicted that the plasma mass would be transported out of the Io plasma torus via the interchange instability, driven by the centrifugal force attributed to the corotational motion (e.g., Ioannidis & Brice, 1971; Siscoe & Summers, 1981; Southwood & Kivelson, 1987, 1989). As a result of this instability, inward moving flux tubes carry the hot and tenuous plasmas originating outside the torus into

the central torus, while outward moving flux tubes carry the cold and dense plasmas of the central torus outside. The net transport of magnetic flux is required to be zero by theoretical consideration of previous studies (Delamere, Otto, et al., 2015). The net transport of the plasma mass is directed outward and is referred to as the mass loading. “Finger”-shaped cross sections on the equatorial plane are formed by the inward and outward moving flux tubes in numerical magnetohydrodynamic (MHD) simulations (e.g., Hiraki et al., 2012; Ma et al., 2016; Wu et al., 2007; Yang et al., 1994), although these shapes are subject to the initial perturbations.

In situ measurements of the magnetic field, plasma waves, and energetic particles actually indicated signatures suggestive of the inward moving flux tubes filled with hot tenuous plasma (Kivelson et al., 1997; Thorne et al., 1997; Russell et al., 2000, 2005). The inward hot plasma transport was also confirmed from radial distribution of hot electron fraction in the torus plasma, which was diagnosed based on extreme ultraviolet (EUV) spectroscopy from the Hisaki satellite (Yoshioka et al., 2014, 2017).

Radially outward transported plasma is finally released from the magnetosphere in some form. The plasmoid ejection via the Vasyliūnas type reconnection in the tail region (Vasyliūnas, 1983) is thought to be the most significant mass release process, despite the still outstanding uncertainty in plasmoid size, density, and total mass (e.g., Cowley et al., 2015; McComas & Bagenal, 2007; McComas et al., 2014; Vogt et al., 2014). Previous studies have reported bursty inward/outward plasma flows in the tail region from midnight to dawn associated with the Vasyliūnas reconnection having a recurrence frequency of 1.5–7 days (e.g., Kasahara et al., 2013; Kronberg et al., 2005, 2007, 2008, 2009; Krupp et al., 1998; Woch et al., 1998, 2002). The previous studies expected that plasma mass release is likely to recur at such a frequency if the bursty inward/outward plasma flows correspond to the plasmoid ejections. It should be noted that the small-scale “drizzle” of plasma on the closed field lines from noon to the dusk side is also one of the mass release candidates (Bagenal, 2007; Delamere, Otto, et al., 2015). In the present study, we refer to the plasmoid ejection in the tail region from midnight to the dawn sector as the “large-scale” Vasyliūnas reconnection to distinguish the small-scale drizzle from noon to the dusk side.

It has long been suggested that the association of the large-scale Vasyliūnas reconnection with “energetic events” is a global disturbance, spreading from the inner to outer magnetosphere (Louarn et al., 2007, 2014, 1998, 2000). During energetic events, transient energetic particle injections and magnetic field perturbations with a duration of a few hours take place in the inner magnetosphere, simultaneously with excitations of the hectometric radio emission emitted from the auroral region and narrow-band kilometric emission emitted from the outer torus. These phenomena recur at a frequency of one event every few days. When the International Ultraviolet Explorer observed variability in the UV aurora like energetic events, thinning of the current sheet, and magnetic field fluctuation around the current sheet crossing were detected in the in situ measurements of Galileo (Prangé et al., 2001). The energetic events highly suggest that the large-scale Vasyliūnas tail reconnection onsets the planetward transport of energy and/or plasma, which are dissipated at the middle magnetosphere, inner magnetosphere, and auroral region.

Recently, continuous monitoring of EUV aurora with Hisaki has indicated that auroral brightening with durations of less than 10 h recur at a frequency of every few days (Kimura et al., 2015, 2017). In this study, a “transient aurora” refers to an impulsive brightening with typical duration less than 10 h. Transient auroral events occurred during periods when the solar wind was relatively quiet. Kimura et al. (2015, 2017) argued that the transient auroral is “internally-driven” by internal plasma supply from Io and Jupiter’s rotation. Auroral imaging by the Hubble space telescope during the transient aurora showed enhancement of poleward auroral structures, which is related to the solar wind interaction, and dawn-storm-like structure (Clarke et al., 2004, 2009; Nichols et al., 2009), which were followed by outer emissions within a few hours (Badman et al., 2016; Gray et al., 2016; Kimura et al., 2017; Nichols et al., 2017). See, for example, Grodent (2015) and Clarke et al. (2004) for details of the poleward aurora, dawn storm, and outer emission. Although there are still controversial discussions on magnetospheric disturbances corresponding to each structure of aurora (e.g., Clarke et al., 2004, 2009; Nichols et al., 2009, 2017), the poleward aurora and dawn storm might be suggestive of magnetopause and tail reconnections, respectively. The outer emissions are highly suggestive of the energetic particle injections (Dumont et al., 2015; Mauk et al., 2002; Radioti et al., 2009). Kimura et al. (2015, 2017) interpreted the transient aurora as a part of the energetic event. The Vasyliūnas reconnection is the most plausible candidate for the initiation of the transient aurora, as

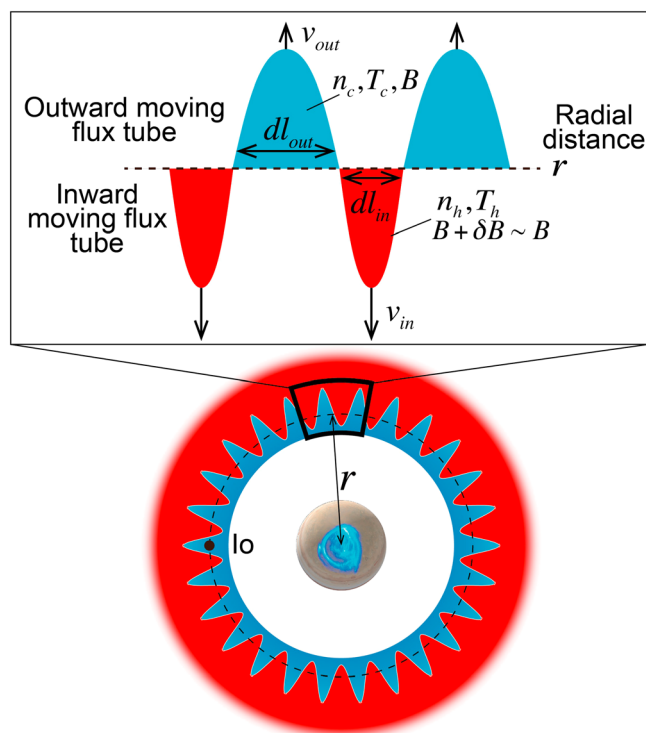


Figure 1. Schematic of the interchange instability in the Io plasma torus. At a radial distance r around Io's orbit, the flux tube with magnetic flux density B is filled with a cold plasma with density n_c at electron temperature T_c . The cold flux tube azimuthally extends with width dl_{out} and moves outward at velocity v_{out} . The hot flux tube with $B + \delta B$, where δB is the difference in the magnetic flux density between the hot and cold flux tubes, filled with a hot tenuous plasma with density n_h at temperature T_h azimuthally extends with width dl_{in} and moves inward at velocity v_{in} .

suggested by the energetic event. Gray et al. (2016) actually indicated that during the transient aurora, an auroral spot merged into the dawn storm from high latitudes, which is suggestive of the reconnection return flow in the outer magnetosphere.

In spite of the circumstantial evidence, it has not been observationally demonstrated that mass release via the Vasyliūnas reconnection should be a consequence of the mass loading.

On 20 January 2015, Kleer and Pater (2016) and Yoneda et al. (2015) found that volcanic eruptions started at Io. This finding is based on the mid-infrared observation of Io's surface and visible observation of the sodium nebula extending around Io's orbit. Hisaki monitored EUV spectrum of torus during the volcanic eruptions and found that the number densities of major ions and electrons in the torus increased up to ~ 2 times greater than pre-eruption values ~ 50 days after the start of volcanic eruptions (Yoshikawa et al., 2017). Yoshikawa et al. (2017) also showed that ~ 20 days after the start of volcanic eruptions, the transient aurora started to recur with a few-day period. This is likely an indication of a mass release process responding to a high mass loading rate associated with volcanic eruptions.

This study proposes a new simple analytical model that can quantitatively estimate the mass loading rate based on continuous monitoring of the EUV luminosity of the torus. Response of the recurrent transient aurora to the estimated mass loading rate is investigated with Hisaki. The recurrent transient aurora is hypothesized to be an indicator of the Vasyliūnas reconnection and also that of the energetic event because these three phenomena are likely "internally driven" with a few-day period by the mass loading from Io and Jupiter's rotation (e.g., Kimura et al., 2015; Louarn et al., 2014; Vasyliūnas, 1983). Based on the auroral response to the estimated mass loading rate, the budget of mass stored in the magnetosphere is discussed.

2. Analytical Model for Plasma Mass Loading Estimation

In the present study, we develop a simple analytical model for estimating the net rate of plasma mass loading based on the torus EUV emission. The torus EUV emission consists of sulfur and oxygen ion emissions sensitive to electron temperature in the torus. One can estimate plasma parameters of torus based on the EUV spectral diagnostics, for example, ion density, cold core electron temperature, and fraction of minor hot electrons. Our new analytical model does not require high spectral resolution UV spectroscopy, as has been required for the spectral diagnostics and physical chemistry models of previous studies (e.g., Yoshioka et al., 2014, 2017). This is because our model associates the total emission power from the torus, not EUV spectral shape, to the mass loading rate (see below). The entire region of the torus EUV emission is spatially integrated to obtain the total emission power. This is possible because the dominant emission region of the torus has a width of $\sim \pm 8 R_J$ (~ 320 arcsec at opposition; R_J = Jovian radius) in the east-west direction from Jupiter and a height of $\sim 2 R_J$ (~ 40 arcsec) in the north-south direction from the centrifugal equator, which are entirely enclosed in the "dumbbell-shaped" slit of the Hisaki EUV spectrometer with an aperture of 140×360 arcsec.

The interchange instability is assumed to take place in the central torus, that is, $\sim 6 R_J$, where magnetic flux tubes filled with hot tenuous plasma move radially inward while those filled with cold dense plasma move radially outward. The system is assumed to be axisymmetric: the rotation axis is aligned with the magnetic axis, and plasma has longitudinally symmetric structure. Figure 1 shows a schematic of the setting. Equatorial cross sections of the inward/outward moving flux tubes have finger- or bubble-like shapes, which are expected from the in situ magnetic field measurements (Kivelson et al., 1997; Thorne et al., 1997). The finger-shape was often set for initial conditions in the MHD simulations (Hiraki et al., 2012; Ma et al., 2016; Wu et al., 2007; Yang et al., 1994). The finger-like shape is displayed in Figure 1.

At a radial distance r around the central torus at $\sim 6 R_J$, a cold dense flux tube with azimuthal width dl_{out} moves outward at radial velocity v_{out} . The cold flux tube is filled with plasma with electron density n_c , electron temperature T_c in energy units, and magnetic flux density B . A hot tenuous flux tube moves inward at radial velocity v_{in} with width dl_{in} , filled with plasma with electron density n_h , electron temperature T_h in energy units, and flux density $B + \delta B$, where δB is the difference in the magnetic flux density between the inward and outward moving flux tubes. All quantities are assumed to be constant in longitude and latitude. The ion and electron densities have the same value at the equatorial plane and exponentially decrease along the background magnetic field lines with a scale height H . The temperature, velocity, and width are spatially uniform along the background field lines within $\pm H$ from the centrifugal equator.

We require the net magnetic flux within a radial distance r to be conserved. This leads to a balance between the magnetic fluxes carried by the inward and outward flows per unit time:

$$Bv_{\text{out}} \oint dl_{\text{out}} = (B + \delta B)v_{\text{in}} \oint dl_{\text{in}} \quad (1)$$

Here the fluxes carried by inward and outward flows are integrated over all longitudes. The integration $\oint dl$ corresponds to the total azimuthal length (or area) of the inward/outward moving flux tube at r . This equation is solved for v_{out} :

$$v_{\text{out}} = v_{\text{in}} \left(1 + \frac{\delta B}{B} \right) \frac{\oint dl_{\text{in}}}{\oint dl_{\text{out}}} = v_{\text{in}} \left(1 + \frac{\delta B}{B} \right) \frac{\oint dl_{\text{in}}}{2\pi r - \oint dl_{\text{in}}} \sim v_{\text{in}} \frac{\oint dl_{\text{in}}}{2\pi r}, \quad (2)$$

which we expand to a first-order Taylor series with $\oint dl_{\text{in}}/2\pi r \ll 1$ and $\delta B/B \ll 1$. The ratio $\oint dl_{\text{in}}/2\pi r \ll 1$ is justified by the in situ magnetic field measurements by Galileo (Kivelson et al., 1997; Russell et al., 2000, 2005), which indicated that the observing time of the inward moving flux tube was less than 1% in total, suggesting a small azimuthal area for the inward moving flux tube. In the present study, we refer to the ratio of the inward flux tube area to the outward flux tube area $\oint dl_{\text{in}}/\oint dl_{\text{out}} \equiv A$ as the “inward/outward (I/O) area ratio.” The flux density difference $\delta B/B \ll 1$ is also justified by the previous studies mentioned above, which showed that the magnetic flux density of the inward moving flux tube is a few percent larger than that of the ambient plasma.

To associate the outward/inward moving flux tubes with the torus EUV emissions, we consider the total energy of hot electrons carried by the inward moving flux tube. The hot electrons are input into the torus through the interchange instability and interact with the ambient electrons and ions via collisional processes, for example, ionization, radiative excitation, and Coulomb interaction. Consequently, EUV photons are emitted from collisionally excited ions. Although the number density fraction of the hot electrons is less than 15% of the ambient torus electron density (e.g., Yoshioka et al., 2014), the input energy of hot electrons contributes to 26–66% of the total EUV emission power (Bagenal & Delamere, 2011). The total input energy of hot electrons is expressed by the inward moving flux tube parameters as

$$W_{\text{in}} = \oint \sqrt{\pi} H n_h T_h v_{\text{in}} dl_{\text{in}} \quad (3)$$

This gives the total azimuthal length of the inward moving flux tube:

$$\oint dl_{\text{in}} = \frac{W_{\text{in}}}{\sqrt{\pi} H n_h T_h v_{\text{in}}} \quad (4)$$

The outward velocity can be associated with the hot electron energy by substituting equation (4) into (2):

$$v_{\text{out}} = \frac{W_{\text{in}}}{2\pi^{3/2} r H n_h T_h} \quad (5)$$

The plasma mass carried by the outward moving flux tube is evaluated as $\sqrt{\pi} H \rho_{\text{out}} \oint v_{\text{out}} dl_{\text{out}}$ where the mass density ρ_{out} is assumed to be dominated by ions with mean mass m_i in a single charge state, resulting in $\rho_{\text{out}} = m_i n_c$. One should note that the inward moving flux tube recirculates the mass inward at a rate of $\sqrt{\pi} H \rho_{\text{in}} \oint v_{\text{in}} dl_{\text{in}}$ with $\rho_{\text{in}} = m_i n_h$, reducing the net rate of plasma mass loading. The net rate of mass loading \dot{M} is rewritten as

$$\dot{M} = \sqrt{\pi} H [\rho_{\text{out}} \oint v_{\text{out}} dl_{\text{out}} - \rho_{\text{in}} \oint v_{\text{in}} dl_{\text{in}}] \quad (6)$$

For the sake of an estimate, we assume that H is the same for the inflow and outflow, recognizing that H is temperature dependent (see, e.g., equation (4) in Delamere et al., 2005). For the temperature-dependent scale height, hot plasma filled in the inward moving flux tube is spread along the field line more broadly than cold plasma in the outward moving flux tube. This would reduce the net rate of \dot{M} in equation (6). Combining equations (1) and (5) with equation (6), \dot{M} is reduced to a simple form:

$$\dot{M} = \frac{m_i W_{in}}{T_h} (n_c/n_h - 1) \quad (7)$$

The inward moving flux tube density n_h was investigated based on the in situ magnetic field measurements by Galileo. Under the assumption of isothermal plasma, Kivelson et al. (1997) and Thorne et al. (1997) estimated the “density differential” $\delta n/n_c = 0.4\text{--}0.47$, which is the density difference between the inward moving flux tube and the ambient plasma, normalized by the ambient plasma density. With the density differential, we obtain the inward moving flux tube density as $n_h = n_c(1 - \delta n/n_c)$, which leads to the final form:

$$\dot{M} = \frac{m_i W_{in}}{T_h} \frac{\delta n/n_c}{(1 - \delta n/n_c)} \quad (8)$$

With $n_h = n_c(1 - \delta n/n_c)$, other essential parameters v_{out} and $A = \oint dl_{in}/\oint dl_{out}$ are rewritten as

$$v_{out} = \frac{W_{in}}{2\pi^{3/2} r H n_c T_h (1 - \delta n/n_c)} \quad (9)$$

and

$$A = \frac{W_{in}}{2\pi^{3/2} r H n_c T_h (1 - \delta n/n_c) v_{in}} \quad (10)$$

We can estimate \dot{M} from the mean ion mass, hot electron temperature, density differential, and total input power of hot electrons. The parameters m_i and T_h have been constrained by the previous EUV spectral diagnostics ($m_i \sim 25$ [amu] and $T_h \sim 100\text{--}400$ [eV]), and W_{in} can be estimated by Hisaki EUV spectroscopy (see details in section 3.2). The most uncertain parameter is $\delta n/n_c$ because there have been only a few estimates from the in situ measurements. In the next section, we constrain $\delta n/n_c$ based on previous studies.

3. Parameter Constraints

3.1. Density Differential and Source Location of Inward Moving Flux Tube

From equation (8), W_{in} is expressed as

$$W_{in} = \frac{\dot{M} T_h (1 - \delta n/n_c)}{m_i \delta n/n_c} \quad (11)$$

Based on this relation, we investigate response of W_{in} with respect to the input parameters \dot{M} and T_h to constrain $\delta n/n_c$. Bagenal and Delamere (2011) constrained W_{in} to 0.2–0.9 TW based on their UV spectral diagnostics from Cassini and Voyager and the physical chemistry model made by Delamere and Bagenal (2003), Delamere et al. (2004), and Steffl et al. (2006). \dot{M} has been estimated to be 0.26–1.4 t/s (1 t = 1,000 kg) based on the physical chemistry model and observations (e.g., Smyth & Marconi, 2003; Saur et al., 2003; Bagenal, 1997; Delamere & Bagenal, 2003; Delamere et al., 2004, 2005). We use a typical temperature of 100–400 eV for T_h , referring to the in situ measurements from Voyager and Galileo (Frank & Paterson, 1999; Sittler & Strobel, 1987) and the remote monitoring and spectral diagnostics from the Hisaki satellite (Yoshioka et al., 2014, 2017; Yoshikawa et al., 2017, 2016).

Figure 2a shows the distribution of W_{in} as a function of \dot{M} and T_h for a density differential $\delta n/n_c = 0.7$. It is evident that some sets of parameters (\dot{M} , T_h , W_{in}) satisfy constraints from previous studies, for example, $W_{in} = 0.9$ TW at $(\dot{M}, T_h) = (1.4 \text{ t/s}, 400 \text{ eV})$. For $\delta n/n_c > 0.7$, the set of parameters is inconsistent with the previous constraints; for example, $W_{in} = 0.9$ TW cannot be derived from the parameter space if $\dot{M} = 0.26\text{--}1.4 \text{ t/s}$ and $T_h = 100\text{--}400 \text{ eV}$. Therefore, we constrain $\delta n/n_c$ to ~ 0.7 as the maximum value. In the same manner, the minimum value of $\delta n/n_c$ is constrained to be ~ 0.35 as shown in Figure 2b. The observed density differential

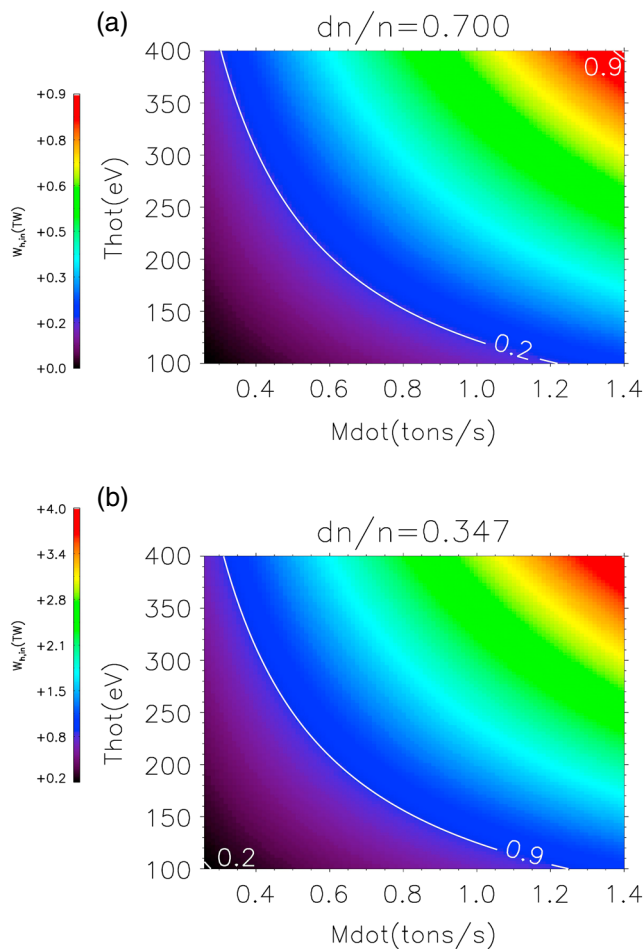


Figure 2. The hot electron energy input to the torus W_{in} as a function of the hot electron temperature T_h and mass loading rate \dot{M} (see equation (11)). (a) W_{in} for a density differential $\delta n/n_c = 0.7$ and (b) that for $\delta n/n_c = 0.35$. The white solid lines show the maximum and minimum values of W_{in} constrained by previous studies ($W_{in} = 0.2, 0.9$).

$\delta n/n_c = 0.4\text{--}0.47$ (Kivelson et al., 1997; Thorne et al., 1997) is between these maximum and minimum values, validating of the assumption and formulation of our analytical model.

We briefly consider the source location of the inward moving flux tube based on the constraint $\delta n/n_c \sim 0.35\text{--}0.7$. Figure 3 shows radial profiles of the equatorial plasma density n and quantity nL^4 associated with the total flux tube content (see, e.g., Siscoe, 1978, for details of the flux tube content). Here the background magnetic field is assumed to be a dipole field. The density profile is the empirical model constructed from the in situ measurements from Galileo and Voyager (Bagenal & Delamere, 2011). The two dotted lines in Figure 3a show hot density profiles with density differentials $\delta n/n_c = 0.35$ and 0.7 , respectively. The quantity nL^4 for hot flux tubes with $\delta n/n_c = 0.35$ and 0.7 is also shown in Figure 3b, represented as dotted lines.

Given that the flux tube content is conserved in the interchange instability, flux tubes with $\delta n/n_c = 0.35$ and 0.7 at $6 R_j$ have the same content as plasmas at 6.7 and $8.0 R_j$, respectively (two intersections of the horizontal broken lines with the solid line in Figure 3b). This indicates that the inward moving flux tube at $6 R_j$ originates from 6.7 to $8.0 R_j$, suggesting that in the torus flux tubes are interchanged with those in the adjacent outer region.

The in situ phase space density measurements of energetic ions by Thorne et al. (1997) suggested that a flux tube with spiky phase space density found at $6.03 R_j$ originates from $6.3 R_j$ if the energetic ions in the flux tube move adiabatically inward. Bagenal and Delamere (2011) showed that the outward transport speed at $L < 10$ is less than 1 km/s , while that at $L > 10$ reaches a few 100 km/s . This implies that transport is diffusive in the central torus and gets advective outside the torus. The diffusive transport is consistent with our concept of adjacently interchanged flux tubes.

3.2. Adopted Parameters

To estimate the plasma mass loading rate, equation (8) is rewritten in practical form:

$$\dot{M} = \frac{m_i}{T_h} \frac{\delta n/n_c}{(1 - \delta n/n_c)} \left[\frac{W_{in}}{W_{total}} \right] \left[\frac{W_{total}}{W_{Hisaki}} \right] W_{Hisaki} \quad (12)$$

where W_{Hisaki} is the total EUV emission power of torus measured with Hisaki, the ratio $[W_{in}/W_{total}]$ is the fraction of the total hot electron input energy to torus emission power for all wavelengths from UV to infrared W_{total} , and the ratio $[W_{total}/W_{Hisaki}]$ is the conversion factor from the power measured with Hisaki to W_{total} .

The present study uses a ratio $[W_{in}/W_{total}] = 0.26$, which is the canonical value adopted by Bagenal and Delamere (2011) from the range $0.26\text{--}0.66$, which was estimated from the energy balance in the physical chemistry model fitted to the Voyager and Cassini observations (Delamere et al., 2004; Delamere & Bagenal, 2003; Steffl et al., 2006). Actually, the ratio $[W_{in}/W_{total}]$ is temporally variable in response to the volcanic activity at Io. However, in the present study we keep the ratio temporally constant for a primary order estimation of mass loading. One should note that the constant $[W_{in}/W_{total}]$ leads to uncertainty in the estimated mass loading. The factor $[W_{total}/W_{Hisaki}]$ is estimated to be 2.1 by taking the ratio of the emission power at $570\text{--}1,460 \text{ \AA}$ to that at $0\text{--}10^4 \text{ \AA}$, modeled by the CHIANTI database with the canonical density and temperature of the torus (see, e.g., Steffl et al., 2004a, 2004b, 2006, 2008, and Yoshioka et al., 2011, 2014, for details of the spectral modeling). Based on the previous section, $\delta n/n_c$ is set to 0.44 , which is the mean of the estimations by Kivelson et al. (1997) and Thorne et al. (1997). The average ion mass m_i is approximately 25 amu with reference to the recent chemical model by Yoshioka et al. (2017).

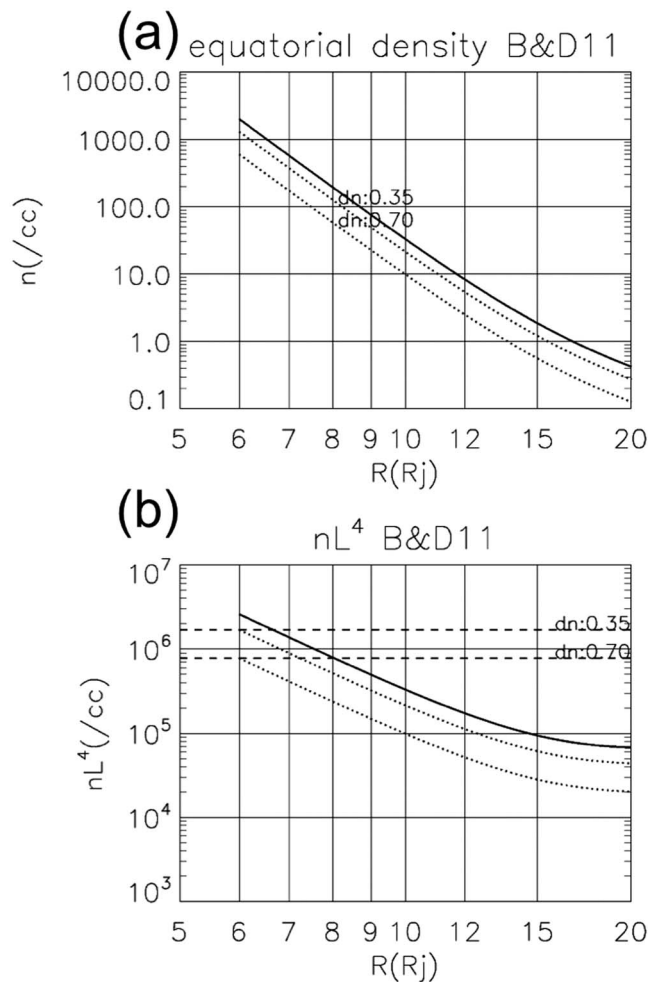


Figure 3. Radial profiles of the equatorial plasma density n and quantity nL^4 that is associated with the total flux tube content. (a) The black line is n as a function of radial distance in Jovian radii adopted from Bagenal and Delamere (2011). The dotted lines are the density profile decreased by the density difference $\delta n/n_c = 0.35$ and 0.7 . (b) The radial profile of nL^4 in a similar format to (a) computed based on n and the dipole field L value. The horizontal broken lines show nL^4 at $6 R_j$ for $\delta n/n_c = 0.35$ and 0.7 .

The hot electron temperature $T_h = 300$ eV is adopted from the range 100–400 eV, estimated from the recent Hisaki observations as referred to above (Yoshikawa et al., 2016, 2017). These adopted parameters are summarized in Table 1.

One should note that some of the input parameters have uncertainties that likely reach several tens of percent with respect to their standard values. The derived mass loading rate also has a similar uncertainty because of the linear propagation of the input parameter uncertainty.

4. Data Set

The Extreme Ultraviolet Spectroscope for Exospheric Dynamics (EXCEED; Yoshioka et al., 2013) onboard Hisaki measures EUV photons from 470 to 1,530 Å, which are reduced to spatio-spectral images with $1,024 \times 1,024$ pixels. Spatial resolution is 17 arcsec, corresponding to $\sim 1 R_j$ around Jupiter's opposition. The "dumbbell-shaped" slit with a width of 360 arcsec in the east–west direction and a thickness of 140 arcsec in the north–south direction was positioned on the northern aurora. The observation period spans from day of year (DOY) –34 to 134 in 2015 (27 November 2014 to 14 May 2015), during which Yoshikawa et al. (2017) discovered enhancements in the torus ion emission that are suggestive of some volcanic eruptions at Io starting around DOY 20. An enhancement in Jupiter's sodium nebula, which is associated with Io's volcanic eruptions, also started to increase on DOY 20 (Kleer & Pater, 2016; Yoneda et al., 2015). Time variations in the emission power of the aurora at 900–1,480 Å were extracted from the imaging spectra, as described in Kimura et al. (2015, 2016, 2017), excluding geocoronal emissions as well as those monitored with Hisaki described in Kuwabara et al. (2017). The torus emission power was extracted from the 570–1,460 Å range in the same manner as the aurora and converted to that at $0\text{--}10^4$ Å. Time resolutions of the aurora and torus power were 10 min.

The solar wind was not monitored near Jupiter during the present observation period. We estimate the solar wind variation at Jupiter using a one-dimensional MHD model that propagates the solar wind measured at the vicinity of Earth (Tao et al., 2005). Uncertainty in the arrival time of the solar wind shock structures, the Corotating Interaction Region and Coronal Mass Ejections, at Jupiter is dependent on the Earth–Sun–Jupiter

angle, which was $82^\circ\text{--}180^\circ$ for the present analysis period. The arrival time uncertainty is estimated to be approximately a few days or more, as discussed in Kimura et al. (2015, 2016), Kita et al. (2016), and Tao et al. (2016a, 2016b).

Table 1

Input Parameters for the Plasma Mass Loading Rate Estimation

	Value	Reference and source
Average ion mass m_i	25 amu	Yoshioka et al. (2017)
Hot electron temperature T_h	300 eV	Yoshikawa et al. (2016)
Density differential $\delta n/n_c$	0.44	Kivelson et al. (1997), Thorne et al. (1997)
Ratio of W_{in} to W_{total} , $[W_{in}/W_{total}]$	0.26	Bagenal and Delamere (2011)
Conversion factor of W_{Hisaki} to W_{total} , $[W_{total}/W_{Hisaki}]$	2.1	Spectra modeled with CHIANTI
Observed EUV power W_{Hisaki}		Observation with Hisaki

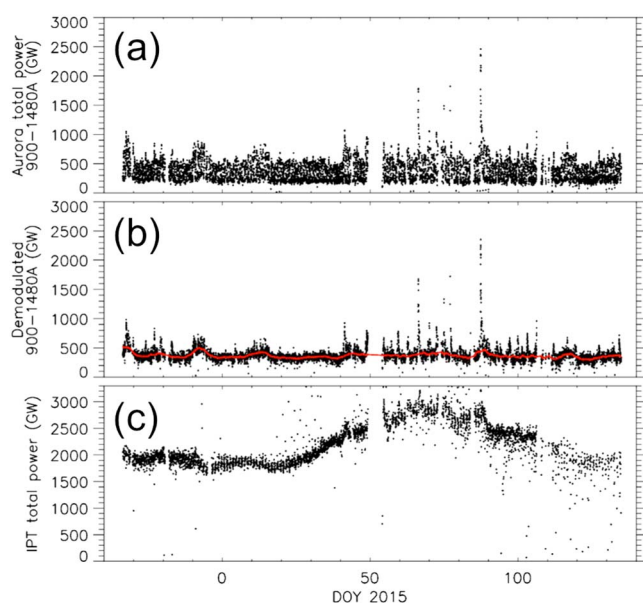


Figure 4. The powers of the EUV emission from the aurora and torus measured by Hisaki. (a) The power of the EUV aurora at 900–1,480 Å. (b) The power demodulated by the sinusoidal function fitting (black dots) and that smoothed by running median with a temporal window of 4 days (red solid line). (c) The total power of the torus emission at 0–10⁴ Å.

5. Data Analysis

5.1. Identification of Transient Aurora

Figure 4 shows the emission powers of the aurora (a) and torus (c) in the present analysis period. The transient aurora is identified by “demodulating” and “detrending” the observed emission power. A sinusoidal function with an offset $A \sin(\Omega_j t) + B$, where t is time, Ω_j is Jupiter’s rotation frequency (2π radians per one planetary rotation, i.e., ~ 0.63 rad/h), and A and B are free parameters, is fitted to the observed emission power (Figure 4a) to model the periodic modulation caused by the corotation of the auroral structure. Subtracting the sinusoidal function $A \sin(\Omega_j t)$ from the observed power demodulates the rotational modulation. The demodulated data (black dots in Figure 4b) have a day-to-day variability associated with the solar wind (see Kita et al., 2016, for the solar wind associated variability) and a variability with typical duration of less than 10 h corresponding to the transient aurora. Long-term variability is extracted from the demodulated data by calculating the running median with a temporal window of 4 days. Subtracting the smoothed data (the red solid line in Figure 4b) from the demodulated data finally derives the detrended data (Figure 5a). The day-to-day (timescales on $>\sim 4$ days) variability associated with the solar wind is suppressed by this processing. From the detrended data, we identify the transient auroras that are maintained for more than 30 min with amplitudes of more than two standard deviations 2σ (the horizontal black solid line in Figure 5a) of the data set. The gray-shaded

periods in Figure 5a are the identified transient auroras. We identified 23 transient auroras in the present analysis period from DOY –34 to 134.

We used the model developed by Tao et al. (2016a, 2016b) to convert the emission power in the 900–1,480 Å range to the corresponding unabsorbed total emission power from the northern hemisphere in the 700–1,800 Å UV range. This removes the effects of Jupiter’s atmospheric absorption and rotational modulation from the data (see Tao et al., 2016a, 2016b, for details). Based on the unabsorbed power, we found that the identified 23 transient auroral events emitted energy of $\sim 10^{15}$ to 10^{17} J/event, which corresponds to total electron energy of $\sim 10^{16}$ to 10^{18} J/event precipitating into the auroral region. The precipitating electron energies are equivalent to ~ 0.1 –10% of the total kinetic energy stored in the corotating magnetospheric plasma, which is thus on the order of $\sim 10^{19}$ J (Bagenal & Delamere, 2011).

5.2. Response of Transient Aurora to Mass Loading Rate

As shown in Figure 5a, the transient auroral power spans 250 (equivalently 2σ) to 2,000 GW, which is 10 times larger than the emission power at periods when no transient aurora is observed. The transient aurora recurs during the period from DOY –34 to –17 followed by a long quiescent period continuing for ~ 60 days. The recurrence restarted on DOY 41 and then continued to DOY 134. The temporal interval between each transient aurora in Figure 5b shows that 2–10 day is the most frequent (21 events) interval. This interval is equivalent to the recurrence frequency of the large-scale Vasyliūnas reconnection and energetic event as discussed in section 1.

The plasma mass loading rate is estimated from equation (12) with the input parameters listed in Table 1. The estimated mass loading rate in Figure 5c shows variability that spans 0.3–0.5 t/s: a moderate decrease from ~ 0.35 t/s to ~ 0.3 t/s on DOY –34 to 20, an increase from ~ 0.3 t/s to a peak at ~ 0.5 t/s on DOY 20–70, a decrease down to ~ 0.35 t/s on DOY 70–125, and finally a small increase up to 0.4 t/s on DOY 125–140. The mass loading enhancement on DOY 20–125 corresponds to several eruptions of volcanoes at Io, as reported by Kleer and Pater (2016). Yoshikawa et al. (2017) indicated an enhancement in the EUV line emissions of sulfur and oxygen ions in multiple charge states. Based on the difference in the temporal evolution between each ion species and charge state, they concluded that neutral gases erupted from Io’s volcanoes on DOY 20–125, as actually detected by Hisaki during this time (Koga et al., 2017), underwent charge exchange

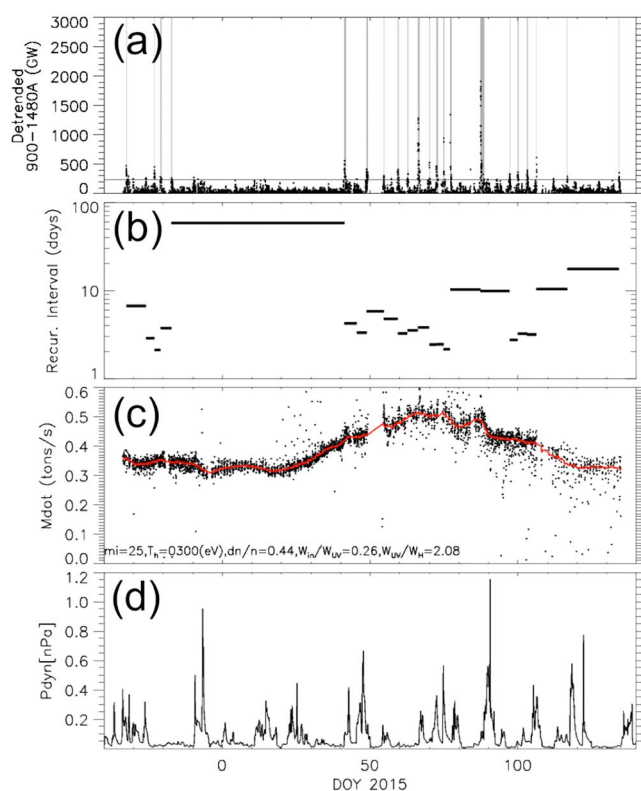


Figure 5. Time series of (a) the emission power and (b) recurrence frequency of the transient aurora, (c) estimated mass loading, and (d) solar wind dynamic pressure in the present analysis period. The gray shades in (a) show the periods when the transient aurora occurred with an amplitude two times larger than the standard deviation of the data set for duration greater than 30 min. The recurrence frequency in (b) is the temporal interval between the onsets of the adjacent transient auroras. The black dot in (c) is the raw mass loading rate estimated with the use of equation (12), and the red solid line is the mass loading rate smoothed by running median with a temporal window of 4 days. The dynamic pressure in (d) is extrapolated from the Earth's orbit by a one-dimensional MHD simulation (Tao et al., 2005).

by Cassini (Tsuchiya et al., 2010), supporting the idea suggested by the present study that the transient aurora is correlated with the solar wind disturbance.

6. Discussion

6.1. Validity of Our Analytical Model

The two-dimensional MHD simulation by Hiraki et al. (2012) reproduced the interchange motion of the equatorial plasma in the plasma torus. Their study indicated an extreme example of radially outward transport via the interchange instability, of which the transport timescale is 2–3 days (Figures 3 and 4 in their paper). In their case, the initial distribution of the radial density profile is limited to 10 l_0 radii, which is much narrower than the actual scale length (approximately some Jovian radii). The interchange instability is strongly amplified by a steep density gradient. Thus, the radial transport timescale of 2–3 days is regarded as an extremely fast case. The timescale of 11–60 days that was observationally estimated by Bagenal and Delamere (2011) and that of 30–40 days was estimated by the radial diffusion model of Copper et al. (2016).

If the plasma torus mass contained in a 10 R_J radius disc, which is approximately the total mass of magnetosphere ~ 1.5 Mt (Bagenal & Delamere, 2011), is transported out of the torus within the 2–3 day period, the mass loading rate corresponds to 1.5–2.1 t/s. Therefore, the mass loading rate is constrained to be less than 2.1 t/s with a transport timescale longer than ~ 2 days. Our estimation from the Hisaki observation is 0.3–0.5 t/s, which is consistently less than the extremely fast case.

and electron impact, and were finally picked up as the ions in the torus. The mass loading rate in the present study shows that picked-up ions provide plasma mass to the magnetosphere during the volcanic event at a relatively higher rate (0.5 t/s) than usual (0.3 t/s).

It is remarkable that the recurrent frequency of the transient aurora is insensitive to the solar wind dynamic pressure (Figure 4d). The 60 day aurora quiescent period spans from DOY -17 to 41 although there are significant spikes in the dynamic pressure. However, there is a significant dependence of aurora on the mass loading. The transient aurora started the frequent recurrence (2–10 day period) on DOY 41 after the mass loading started to increase. The recurrence stopped for ~ 20 days in the end of mass loading decrease around DOY 120. The disappearance of the recurrent aurora on DOY -17 could also be associated with the decrease in the mass loading from DOY -34 to DOY 0. These observational results do not contradict implications that the transient aurora and energetic event are likely associated with the mass loading and are basically independent of the solar wind; that is, they are “internally driven” processes, as recently argued in Kimura et al. (2015, 2017) and other studies.

However, we suggest that there is an exceptional correspondence between the transient aurora and the solar wind. The transient aurora with a peak power of ~ 2 TW, which is the strongest auroral power in the present analysis period, occurs during the interplanetary shock arrival at Jupiter on DOY 87. The unabsorbed emission power of the peak is estimated to be ~ 10 TW by the Tao et al. (2016a, 2016b) model. The temporal intervals between the strongest event and adjacent transient auroras are ~ 10 days, which are longer than the most frequent interval of 2–6 days. This correspondence implies that the transient aurora is, in some cases, forced to occur due to the solar wind disturbance. On DOY 142 in 2017, when Juno detected a solar wind forward shock arriving at Jupiter, Hisaki observed the transient aurora with one of the largest peak powers that has been measured through the entire Hisaki observing period from November 2013 to July 2016 (Kimura et al., 2017; Nichols et al., 2017). This solar wind associated brightening was also fragmentally observed

In the present analysis period, the outward transport velocity v_{out} is estimated to be 25–40 m/s from equation (9) with the parameters presented in Table 1, cold plasma density $n_c = 2,000/\text{cm}^3$, scale height $H = 1 R_j$, and radial distance $r = 6 R_j$. Parameter v_{out} peaked at 40 m/s on DOY 70 when the mass loading rate also reached a maximum. This is naturally consistent with the outward velocity of 20–100 m/s at $6 R_j$ previously estimated from in situ observations and the physical chemistry model by Bagenal and Delamere (2011) and Yoshioka et al. (2017).

The I/O area ratio A is estimated to be 0.5–0.8% from equation (10) with the parameters presented in Table 1, $n_c = 2,000/\text{cm}^3$, $H = 1 R_j$, $r = 6 R_j$, and $v_{\text{in}} = 5 \text{ km/s}$. Yoshikawa et al. (2016) estimated the inward moving velocity of hot electrons v_{in} to be 2–12 km/s under the assumption of hot electron temperature at 100–400 eV.

Here we assume again that the scale heights of the inward and outward moving flux tubes are of the same quantity. This leads to v_{out} and I/O area ratio greater than those with the temperature-dependent scale height.

The given inward velocity of 5 km/s also agrees with another estimation by Russell et al. (2005), who inferred a velocity of a few kilometers per second from magnetic field measurements of the hot inward moving flux tube. They assumed that the occurrence frequency of the inward moving flux tube is equivalent to the fraction of the azimuthal area of the inward moving flux, as described in section 2 of the present study. Assuming conservation of magnetic flux, they estimated v_{in} to be a few kilometers per second for a canonical mass loading rate of 1 t/s, with an I/O area ratio of 0.3%. Thus, we adopt $v_{\text{in}} = 5 \text{ km/s}$ in this discussion. Our resultant A of 0.5–0.8% is comparable with the estimation of 0.3% by Russell et al. (2005). It should be noted that in the present analysis period, A increased from 0.5% up to 0.8% as the mass loading rate increased. Under the assumption of a constant v_{in} , this implies that the inward moving flux tube occurred more frequently due to the higher volcanic activity.

Thorne et al. (1997) estimated the inward velocity to be $\sim 100 \text{ km/s}$ based on the in situ measurements of magnetic field and kiloelectronvolt particle by Galileo. However, this estimation does not agree with the inward velocity of a few kilometers per second recently estimated from the dynamics and distribution of hot electron at 100–400 eV observed from Hisaki (Yoshikawa et al., 2016; Yoshioka et al., 2017). Here we keep adopting the inward velocity of a few kilometers per second to ensure consistency with the recent Hisaki observation by Yoshikawa et al. (2016) and Yoshioka et al. (2017).

Based on the above discussion, we conclude that the present estimation of the three quantities, \dot{M} , v_{out} , and A , are consistent with previous observations and theories. This justifies the assumptions and formulations of our analytical model.

6.2. Plasma Mass Accumulated in Magnetosphere

We estimate the total mass accumulated in the magnetosphere from the observed mass loading rate, shown with the solid black line in Figure 6a. The observed mass loading rate is temporally integrated from the time when the transient aurora dimmed out on DOY –15. Here it is assumed that there is no mass release from the magnetosphere. It should be noted that plasma mass was already accumulating in the magnetosphere before the starting time of integration. The present analysis just indicates a difference in the cumulative mass from the epoch. One should also note that mass release by the drizzle is not considered here for simplicity. Therefore, our estimated cumulative mass is potentially overestimated.

When the transient aurora recurred again on DOY 41 after the quiescent period, the cumulative mass reached the total mass of the magnetosphere, $\sim 1.5 \text{ Mt}$, which is comparable with that estimated from the radial profile of mass density measured by the in situ observations (Bagenal & Delamere, 2011). Although it is still unclear what magnetospheric disturbance corresponds to the transient aurora, if we suppose the transient aurora is an indicator of plasmoid ejection via the large-scale Vasyliūnas reconnection, the recurrence of plasmoid ejection likely requires the “precondition” that the amount comparable to the total mass of magnetosphere is supplied from the torus.

6.3. Balance Between Mass Loading and Plasmoid Ejection

Jupiter’s magnetosphere likely releases the plasma mass via the processes introduced in section 1. The recurrent plasmoid ejection associated with the large-scale Vasyliūnas reconnection has been thought to be the

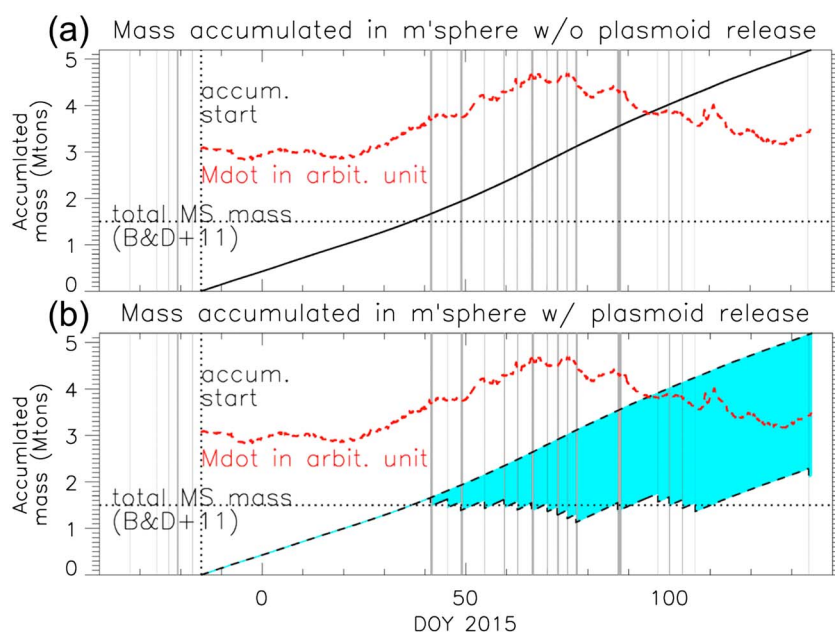


Figure 6. (a) Total mass accumulated in the magnetosphere without mass release process. The black solid line is the total mass temporally integrated from the epoch on DOY -15 , shown with the black vertical dotted line. The gray shades show intervals when the transient auroras were observed. The estimated mass loading rate is shown with the red broken line in arbitrary units. The black horizontal dotted line shows the total mass of magnetosphere (Bagenal & Delamere, 2011). (b) Total mass accumulated in the magnetosphere with mass release via plasmoid ejection in the same format as (a). The upper black broken line shows the cumulative mass with mass release via recurrent plasmoid release at a rate of 28 t/plasmoid, while the bottom black broken line shows the mass with release at a rate of 0.14 Mt/plasmoid.

most significant mass release process in previous studies (e.g., Kronberg et al., 2005, 2007, 2008, 2009; Krupp et al., 1998; Vasyliūnas, 1983; Woch et al., 1998). However, the contribution of the plasmoid ejection to the total mass balance of the magnetosphere is still a big open question, mainly because of the large uncertainty in the plasmoid mass.

Recent studies estimated the plasmoid mass with different sizes and occurrence frequencies based on the in situ observations of reconnection sites ($\sim 100 R_j$; Bagenal, 2007; Kronberg et al., 2008; McComas et al., 2014; Vogt et al., 2014), ranging from 28 to $\sim 10,000$ t. With these plasmoid masses, the temporally averaged rate of mass release from the magnetosphere reaches only 120 kg/s or less, which does not balance the typical mass loading rate of 0.26–1.4 t/s. Bagenal (2007) and Delamere, Otto, et al. (2015) proposed the small-scale “drizzle” process to resolve the discrepancy between the mass loss and source rates.

Cowley et al. (2015) attributed the discrepancy to small plasmoid sizes from 230 to $\sim 20,000 R_j^3$. They modified the size to a larger value by introducing a flux tube stretching process in the distant tail region. In the modification, they referred to the global MHD simulation by Fukazawa et al. (2010), which indicated the creation of large plasmoids with $\sim 300 R_j$ cross-tail length and $\sim 25 R_j$ radius in the nightside meridian plane, that is, a volume of $6 \times 10^5 R_j^3$. This large plasmoid is consistent with those discovered by the in situ observations of a distant tail region of $> 500 R_j$ by New Horizons (McComas & Bagenal, 2007). With a size of $6 \times 10^5 R_j^3$, density of $0.02/\text{cm}^3$ and particle mass of 20 amu in the tail region (Fukazawa et al., 2010), the plasmoid mass is approximately 0.14 Mt (1.4×10^5 t).

In the present analysis, we investigate the balance between the mass release via the heavy plasmoid ejection and the mass loading. Here the plasmoid is assumed to be ejected from the magnetosphere simultaneously as the transient aurora, followed by the recurrent reduction of the cumulative mass. The black broken lines in Figure 6b show the mass balance in the same format as Figure 6a. The upper broken line is estimated with a plasmoid mass of 28 t while the bottom line is estimated with a mass of 0.14 Mt. The light blue region shows a possible range of cumulative mass. It should be noted that for plasmoid ejections of 0.14 Mt, the cumulative mass is suppressed down to the total mass of magnetosphere on DOY 40–106, while the ejections of 28 ton

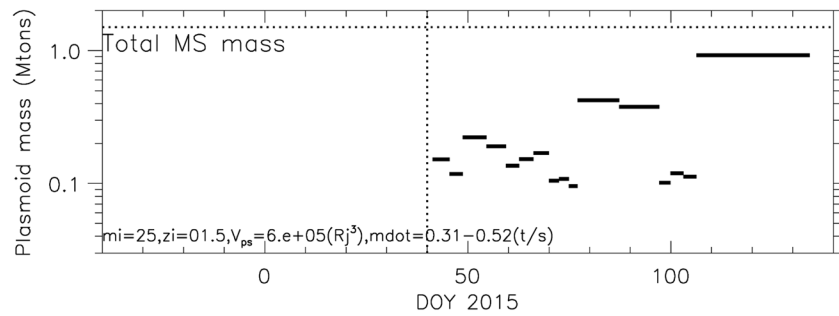


Figure 7. Plasmoid mass estimated from temporal interval of the transient aurora and mass loading rate. The plasmoid mass ΔM at time of transient aurora is given by the temporal integration of the mass loading rate $\Delta M(t_2) = \int_{t_1}^{t_2} \dot{M}(t) dt$, where $\dot{M}(t)$ is the mass loading as function of time, t_1 is starting time of the previous transient aurora, and t_2 is transient aurora of interest. Horizontal thick black bars show the estimated ΔM corresponding to each transient aurora that occurred at the right edge of the black bar.

shows insignificant contribution to the mass loss. Although it is unclear whether recurrence of plasmoid ejection restarted from DOY 134 due to lack of observations, the recurrence of plasmoid could restart after ~ 0.9 Mt was accumulated throughout the long quiescent period on DOY 106–134.

Variability in plasmoid mass is also investigated under the assumption that plasma mass loading during the temporal interval between two adjacent transient auroras is entirely ejected at the time of the subsequent transient aurora. In other words, the total mass of the magnetosphere is assumed to be constant by plasmoid ejections with the variable mass. Figure 7 shows the variable plasmoid mass $\Delta M(t_2)$ at plasmoid ejection time t_2 , which is estimated from the temporal integration of the mass loading rate $\Delta M(t_2) = \int_{t_1}^{t_2} \dot{M}(t) dt$, where $\dot{M}(t)$ is the mass loading as function of time, t_1 is starting time of the previous transient aurora, and t_2 is the starting time of the subsequent transient aurora. The variability in plasmoid mass during DOY 41–106 spans from 0.09 to 0.5 Mt.

Based on the discussion regarding temporally constant and variable plasmoid masses, we conclude that a plasmoid mass greater than ~ 0.1 Mt is necessary in case that the recurrent plasmoid ejection is the only process for mass release.

7. Summary

We developed an analytic method for estimating the mass loading at Jupiter based on the interchange instability in the Io torus. This analytic model was used to constrain the parameters associated with the interchange instability:

1. According to previous in situ measurements and a physical chemistry model, the density differential of the inward moving flux tube $\delta n/n_c$ was constrained to be 0.35–0.7.
2. The constrained density differential suggests that in the torus flux tubes are interchanged with those in the adjacent outer region; for example, a flux tube at $6 R_j$ is likely interchanged with that at $6.7\text{--}8 R_j$.

Following our analytic model, the mass loading rate was estimated from the torus EUV monitoring during Io's volcanic eruptions in 2015 and compared with the transient aurora. We obtained the following observation results:

3. Mass loading rate varied over a range of 0.3–0.5 t/s during the volcanic eruptions on DOY 20–125.
4. During the relatively low mass loading period of DOY –17 to 41, the transient aurora dimmed out even at the solar wind shock arrival.
5. During the relatively high mass loading period of DOY 41–125, the transient aurora indicated the recurrence typically at a 2–6 day period.
6. There was an exceptional transient auroral event with an emission power of 10 TW around the solar wind shock arrival at Jupiter on DOY 87.
7. Energies equivalent to 0.1–10% of the total kinetic energy stored in the corotating magnetospheric plasma are input to each transient aurora.

Based on the observation results, we speculate the circulation and release of plasma mass:

8. The I/O area ratio and outward moving flux speed likely varied over ranges of 0.5–0.8% and 25–40 m/s in correlation with the mass loading rate, respectively.
9. The recurrence of plasmoid ejection requires the precondition that the amount comparable to the total mass of magnetosphere, ~1.5 Mt, is carried out of the torus.
10. A large plasmoid mass greater than 0.1 Mt is necessary in case that the recurrent plasmoid ejection is the only process for mass release.

Acknowledgments

The data of Hisaki satellite is archived in the Data Archives and Transmission System (DARTS) JAXA (<https://www.darts.isas.jaxa.jp/stp/hisaki/>). Users can access the data in DARTS directly. T.K. was supported by a Grant-in-Aid for Scientific Research (16K17812) from the Japan Society for the Promotion of Science (JSPS). The authors acknowledge the support of the International Space Science Institute (ISSI), as this study was discussed within ISSI International Team "The influence of Io on Jupiter's magnetosphere." T.K. would like to thank A. Steffl for fruitful discussions throughout this study. This work was supported by JSPS and MAEDI under the Japan-France Integral Action Program (SAKURA).

References

- Achilleos, N., André, N., Blanco-Cano, X., Brandt, P. C., Delamere, P. A., & Winglee, R. (2014). 1. Transport of mass, momentum and energy in planetary magnetodisc regions. *Space Science Reviews*, 187(1–4), 229–299. <https://doi.org/10.1007/s11214-014-0086-y>
- Badman, S. V., Bonfond, B., Fujimoto, M., Gray, R. L., Kasaba, Y., Kasahara, S., et al. (2016). Weakening of Jupiter's main auroral emission during January 2014. *Geophysical Research Letters*, 43, 988–997. <https://doi.org/10.1002/2015GL067366>
- Bagenal, F. (1997). The ionization source near Io from Galileo wake data. *Geophysical Research Letters*, 24, 2111–2114.
- Bagenal, F. (2007). The magnetosphere of Jupiter: Coupling the equator to the poles. *Journal of Atmospheric and Solar: Terrestrial Physics*, 69(3), 387–402. <https://doi.org/10.1016/j.jastp.2006.08.012>
- Bagenal, F., & Delamere, P. A. (2011). Flow of mass and energy in the magnetospheres of Jupiter and Saturn. *Journal of Geophysical Research*, 116, A05209. <https://doi.org/10.1029/2010JA016294>
- Bagenal, F., Dowling, T., & McKinnon, B. (Eds.) (2004). *Jupiter: Planet, Satellites, Magnetosphere*. Cambridge, UK: Cambridge University Press.
- Clarke, J. T., Grodent, D., Cowley, S., Bunce, E., Connerney, J., & Satoh, T. (2004). Jupiter's aurora. In F. Bagenal, T. E. Dowling, & W. B. McKinnon (Eds.), *Jupiter. The Planet, Satellites and Magnetosphere* (pp. 639–670). Cambridge, UK: Cambridge University Press.
- Clarke, J. T., Nichols, J., Gérard, J. C., Grodent, D., Hansen, K. C., Kurth, W., et al. (2009). Response of Jupiter's and Saturn's auroral activity to the solar wind. *Journal of Geophysical Research*, 114, A05210. <https://doi.org/10.1029/2008JA013694>
- Copper, M., Delamere, P. A., & Overcast-Howe, K. (2016). Modeling physical chemistry of the Io plasma torus in two dimensions. *Journal of Geophysical Research: Space Physics*, 121, 6602–6619. <https://doi.org/10.1002/2016JA022767>
- Cowley, S. W. H., Nichols, J. D., & Jackman, C. M. (2015). Down-tail mass loss by plasmoids in Jupiter's and Saturn's magnetospheres. *Journal of Geophysical Research: Space Physics*, 120, 6347–6356. <https://doi.org/10.1002/2015JA021500>
- Delamere, P. A., & Bagenal, F. (2003). Modeling variability of plasma conditions in the Io torus. *Journal of Geophysical Research*, 108(A7), 1276. <https://doi.org/10.1029/2002JA009706>
- Delamere, P. A., Bagenal, F., Paranicas, C., Masters, A., Radioti, A., Bonfond, B., et al. (2015). Solar wind and internally driven dynamics: Influences on magnetodiscs and auroral responses. *Space Science Reviews*, 187(1–4), 51–97. <https://doi.org/10.1007/s11214-014-0075-1>
- Delamere, P. A., Bagenal, F., & Steffl, A. (2005). Radial variations in the Io plasma torus during the Cassini era. *Journal of Geophysical Research*, 110, A12223. <https://doi.org/10.1029/2005JA011251>
- Delamere, P. A., Otto, A., Ma, X., Bagenal, F., & Wilson, R. J. (2015). Magnetic flux circulation in the rotationally driven giant magnetospheres. *Journal of Geophysical Research: Space Physics*, 120, 4229–4245. <https://doi.org/10.1002/2015JA021036>
- Delamere, P. A., Steffl, A., & Bagenal, F. (2004). Modeling temporal variability of plasma conditions in the Io torus during the Cassini era. *Journal of Geophysical Research*, 109, A10216. <https://doi.org/10.1029/2003JA010354>
- Dumont, M., Grodent, D., Radioti, A., Bonfond, B., & Gérard, J.-C. (2015). Jupiter's equatorward auroral features: Possible signatures of magnetospheric injections. *Journal of Geophysical Research: Space Physics*, 119, 10,068–10,077. <https://doi.org/10.1002/2014JA020527>
- Frank, L. A., & Paterson, W. R. (1999). Intense electron beams observed at Io with the Galileo spacecraft. *Journal of Geophysical Research*, 104(A12), 28,657–28,669. <https://doi.org/10.1029/1999JA900402>
- Fukazawa, K., Ogino, T., & Walker, R. J. (2010). A simulation study of dynamics in the distant Jovian magnetotail. *Journal of Geophysical Research*, 115, A09219. <https://doi.org/10.1029/2009JA015228>
- Gray, R. L., Badman, S. V., Bonfond, B., Kimura, T., Misawa, H., Nichols, J. D., et al. (2016). Auroral evidence of radial transport at Jupiter during January 2014. *Journal of Geophysical Research: Space Physics*, 121, 9972–9984. <https://doi.org/10.1002/2016JA023007>
- Grodent, D. (2015). A brief review of ultraviolet auroral emissions on giant planets. *Space Science Reviews*, 187(1–4), 23–50. <https://doi.org/10.1007/s11214-014-0052-8>
- Hiraki, Y., Tsuchiya, F., & Katoh, Y. (2012). Io torus plasma transport under interchange instability and flow shears. *Planetary and Space Science*, 62(1), 41–47. <https://doi.org/10.1016/j.pss.2011.11.014>
- Ioannidis, G., & Brice, N. (1971). Plasma densities in the Jovian magnetosphere: Plasma slingshot or Maxwell demon. *Icarus*, 14(3), 360–373. [https://doi.org/10.1016/0019-1035\(71\)90007-8](https://doi.org/10.1016/0019-1035(71)90007-8)
- Kasahara, S., Kronberg, E. A., Kimura, T., Tao, C., Badman, S. V., Masters, A., et al. (2013). Asymmetric distribution of reconnection jet fronts in the Jovian nightside magnetosphere. *Journal of Geophysical Research: Space Physics*, 118, 375–384. <https://doi.org/10.1029/2012JA018130>
- Kimura, T., Badman, S. V., Tao, C., Yoshioka, K., Murakami, G., Yamazaki, A., et al. (2015). Transient internally driven aurora at Jupiter discovered by Hisaki and the Hubble space telescope. *Geophysical Research Letters*, 42, 1662–1668. <https://doi.org/10.1002/2015GL063272>
- Kimura, T., Kraft, R. P., Elsner, R. F., Branduardi-Raymont, G., Gladstone, G. R., Tao, C., et al. (2016). Jupiter's X-ray and EUV auroras monitored by Chandra, XMM-Newton, and Hisaki satellite. *Journal of Geophysical Research: Space Physics*, 121, 2308–2320. <https://doi.org/10.1002/2015JA021893>
- Kimura, T., Nichols, J. D., Gray, R. L., Tao, C., Murakami, G., Yamazaki, A., et al. (2017). Transient brightening of Jupiter's aurora observed by the Hisaki satellite and Hubble space telescope during approach phase of the Juno spacecraft, special issue 'early results: Juno at Jupiter'. *Geophysical Research Letters*, 44, 4523–4531. <https://doi.org/10.1002/2017GL072912>
- Kita, H., Kimura, T., Tao, C., Tsuchiya, F., Misawa, H., Sakanoi, T., et al. (2016). Characteristics of solar wind control on Jovian UV auroral activity deciphered by long-term Hisaki EXCEED observations: Evidence of preconditioning of the magnetosphere? *Geophysical Research Letters*, 43, 6790–6798. <https://doi.org/10.1002/2016GL069481>
- Kivelson, M. G. (2014). Planetary magnetodiscs: Some unanswered questions. *Space Science Reviews*, 187(1–4), 5–21. <https://doi.org/10.1007/s11214-014-0046-6>
- Kivelson, M. G., Khurana, K. K., Russell, C. T., & Walker, R. J. (1997). Intermittent short-duration magnetic field anomalies in the Io torus: Evidence for plasma interchange? *Geophysical Research Letters*, 24(17), 2127–2130. <https://doi.org/10.1029/97GL02202>

- Kleer, d., & Pater, d. (2016). Time variability of Io's volcanic activity from near-IR adaptive optics observations on 100 nights in 2013–2015. *Icarus*, 280, 378–404. <https://doi.org/10.1016/j.icarus.2016.06.019>
- Koga, R., Tsuchiya, F., Kagitani, M., Sakanoi, T., Yoneda, M., Yoshioka, K., et al. (2017). The time variation of atomic oxygen emission around Io during a volcanic event observed with Hisaki/EXCEED. *Icarus*, 299, 300–307
- Kronberg, E. A., Glassmeier, K.-H., Woch, J., Krupp, N., Lagg, A., & Dougherty, M. K. (2007). A possible intrinsic mechanism for the quasi-periodic dynamics of the Jovian magnetosphere. *Journal of Geophysical Research*, 112, A05203. <https://doi.org/10.1029/2006JA011994>
- Kronberg, E. A., Woch, J., Krupp, N., & Lagg, A. (2009). A summary of observational records on periodicities above the rotational period in the Jovian magnetosphere. *Annales Geophysique*, 27, 2565–2573. <https://doi.org/10.5194/angeo-27-2565-2009>
- Kronberg, E. A., Woch, J., Krupp, N., Lagg, A., Daly, P. W., & Korth, A. (2008). Comparison of periodic substorms at Jupiter and Earth. *Journal of Geophysical Research*, 113, A04212. <https://doi.org/10.1029/2007JA012880>
- Kronberg, E. A., Woch, J., Krupp, N., Lagg, A., Khurana, K. K., & Glassmeier, K.-H. (2005). Mass release at Jupiter: Substorm-like processes in the Jovian magnetotail. *Journal of Geophysical Research*, 110, A03211. <https://doi.org/10.1029/2004JA010777>
- Krupp, N., Woch, J., Lagg, A., Wilken, B., Livi, S., & Williams, D. J. (1998). Energetic particle bursts in the predawn Jovian magnetotail. *Geophysical Research Letters*, 25, 1249–1252. <https://doi.org/10.1029/98GL00863>
- Kuwabara, M., Yoshioka, K., Murakami, G., Tsuchiya, F., Kimura, T., Yamazaki, A., & Yoshikawa, I. (2017). The geocoronal responses to the geomagnetic disturbances. *Journal of Geophysical Research: Space Physics*, 122, 1269–1276. <https://doi.org/10.1002/2016JA023247>
- Louarn, P., Kurth, W. S., Gurnett, D. A., Hospodarsky, G. B., Persoon, A. M., Cecconi, B., et al. (2007). Observation of similar radio signatures at Saturn and Jupiter: Implications for the magnetospheric dynamics. *Geophysical Research Letters*, 34, L20113. <https://doi.org/10.1029/2007GL030368>
- Louarn, P., Paranicas, C. P., & Kurth, W. S. (2014). Global magnetodisk disturbances and energetic particle injections at Jupiter. *Journal of Geophysical Research: Space Physics*, 119, 4495–4511. <https://doi.org/10.1002/2014JA019846>
- Louarn, P., Roux, A., Perraut, S., Kurth, W., & Gurnett, D. (1998). A study of the large-scale dynamics of the jovian magnetosphere using the Galileo plasma wave experiment. *Geophysical Research Letters*, 25(15), 2905–2908. <https://doi.org/10.1029/98GL01774>
- Louarn, P., Roux, A., Perraut, S., Kurth, W. S., & Gurnett, D. A. (2000). A study of the Jovian “energetic magnetospheric events” observed by Galileo: Role in the radial plasma transport. *Journal of Geophysical Research*, 105(A6), 13,073–13,088. <https://doi.org/10.1029/1999JA900478>
- Ma, X., Delamere, P. A., & Otto, A. (2016). Plasma transport driven by the Rayleigh-Taylor instability. *Journal of Geophysical Research: Space Physics*, 121, 5260–5271. <https://doi.org/10.1002/2015JA022122>
- Mauk, B. H., Clarke, J. T., Grodent, D., Waite, J. H., Paranicas, C. P., & Williams, D. J. (2002). Transient aurora on Jupiter from injections of magnetospheric electrons. *Nature*, 415(6875), 1003–1005. <https://doi.org/10.1038/4151003a>
- McComas, D. J., & Bagenal, F. (2007). Jupiter: A fundamentally different magnetospheric interaction with the solar wind. *Geophysical Research Letters*, 34, L20106. <https://doi.org/10.1029/2007GL031078>
- McComas, D. J., Bagenal, F., & Ebert, R. W. (2014). Bimodal size of Jupiter's magnetosphere. *Journal of Geophysical Research: Space Physics*, 119, 1523–1529. <https://doi.org/10.1002/2013JA019660>
- Nichols, J. D., Badman, S. V., Bagenal, F., Bolton, S. J., Bonfond, B., Bunce, E. J., et al. (2017). Response of Jupiter's auroras to conditions in the interplanetary medium as measured by the Hubble space telescope and Juno. *Geophysical Research Letters*, 44, 7643–7652. <https://doi.org/10.1002/2017GL073029>
- Nichols, J. D., Clarke, J. T., Gérard, J.-C., Grodent, D., & Hansen, K. C. (2009). Variation of different components of Jupiter's auroral emission. *Journal of Geophysical Research*, 114, A06210. <https://doi.org/10.1029/2009JA014051>
- Prangé, R., Chagnon, G., Kivelson, M. G., Livengood, T. A., & Kurth, W. (2001). Temporal monitoring of Jupiter's auroral activity with IUE during the Galileo mission. Implications for magnetospheric processes. *Planetary and Space Science*, 49(3–4), 405–415. [https://doi.org/10.1016/S0032-0633\(00\)00161-6](https://doi.org/10.1016/S0032-0633(00)00161-6)
- Radioti, A., Tomás, A. T., Grodent, D., Gérard, J.-C., Gustin, J., Bonfond, B., et al. (2009). Equatorward diffuse auroral emissions at Jupiter: Simultaneous HST and Galileo observations. *Geophysical Research Letters*, 36, L07101. <https://doi.org/10.1029/2009GL037857>
- Russell, C. T., Kivelson, M. G., & Khurana, K. K. (2005). Statistics of depleted flux tubes in the Jovian magnetosphere. *Planetary and Space Science*, 53(9), 937–943. <https://doi.org/10.1016/j.pss.2005.04.007>
- Russell, C. T., Kivelson, M. G., Khurana, K. K., & Huddleston, D. E. (2000). Circulation and dynamics in the Jovian magnetosphere. *Advances in Space Research*, 26(10), 1671–1676. [https://doi.org/10.1016/S0273-1177\(00\)00115-0](https://doi.org/10.1016/S0273-1177(00)00115-0)
- Saur, J., Strobel, D. F., Neubauer, F. M., & Summers, M. E. (2003). The ion mass loading rate at Io. *Icarus*, 163(2), 456–468. [https://doi.org/10.1016/S0019-1035\(03\)00085-X](https://doi.org/10.1016/S0019-1035(03)00085-X)
- Siscoe, G. L. (1978). Jovian plasmaspheres. *Journal of Geophysical Research*, 83(A5), 2118–2126. <https://doi.org/10.1029/JA083iA05p02118>
- Siscoe, G. L., & Summers, D. (1981). Centrifugally driven diffusion of iogenic plasma. *Journal of Geophysical Research*, 86(A10), 8471–8479. <https://doi.org/10.1029/JA086iA10p08471>
- Sittler, E. C. Jr., & Strobel, D. F. (1987). Io plasma torus electrons: Voyager 1. *Journal of Geophysical Research*, 92(A6), 5741–5762. <https://doi.org/10.1029/JA092iA06p05741>
- Smyth, W. H., & Marconi, M. L. (2003). Nature of the iogenic plasma source in Jupiter's magnetosphere I. Circumplanetary distribution. *Icarus*, 166(1), 85–106. [https://doi.org/10.1016/S0019-1035\(03\)00176-3](https://doi.org/10.1016/S0019-1035(03)00176-3)
- Southwood, D. J., & Kivelson, M. G. (1987). Magnetospheric interchange instability. *Journal of Geophysical Research*, 92(A1), 109. <https://doi.org/10.1029/JA092iA01p0109>
- Southwood, D. J., & Kivelson, M. G. (1989). Magnetospheric interchange motions. *Journal of Geophysical Research*, 94(A1), 299–308. <https://doi.org/10.1029/JA094iA01p00299>
- Steffl, A. J., Bagenal, F., & Stewart, A. I. F. (2004a). Cassini UVIS observations of the Io plasma torus: I. Initial results. *Icarus*, 172(1), 78–90. <https://doi.org/10.1016/j.icarus.2003.12.027>
- Steffl, A. J., Bagenal, F., & Stewart, A. I. F. (2004b). Cassini UVIS observations of the Io plasma torus. II. Radial variations. *Icarus*, 172(1), 91–103. <https://doi.org/10.1016/j.icarus.2004.04.016>
- Steffl, A. J., Delamere, P. A., & Bagenal, F. (2006). Cassini UVIS observations of the Io plasma torus. III. Modeling temporal and azimuthal variability. *Icarus*, 180(1), 124–140. <https://doi.org/10.1016/j.icarus.2005.07.013>
- Steffl, A. J., Delamere, P. A., & Bagenal, F. (2008). Cassini UVIS observations of the Io plasma torus. IV. Observations of temporal and azimuthal variability. *Icarus*, 194(1), 153–165. <https://doi.org/10.1016/j.icarus.2007.09.019>
- Tao, C., Kataoka, R., Fukunishi, H., Takahashi, Y., & Yokoyama, T. (2005). Magnetic field variations in the Jovian magnetotail induced by solar wind dynamic pressure enhancements. *Journal of Geophysical Research*, 110, A11208. <https://doi.org/10.1029/2004JA010959>

- Tao, C., Kimura, T., Badman, S. V., André, N., Tsuchiya, F., Murakami, G., et al. (2016a). Variation of Jupiter's aurora observed by Hisaki/EXCEED: 2. Estimations of auroral parameters and magnetospheric dynamics. *Journal of Geophysical Research: Space Physics*, 121, 4055–4071. <https://doi.org/10.1002/2015JA021272>
- Tao, C., Kimura, T., Badman, S. V., André, N., Tsuchiya, F., Murakami, G., et al. (2016b). Variation of Jupiter's aurora observed by Hisaki/EXCEED: 1. Observed characteristics of the auroral electron energies compared with observations performed using HST/STIS. *Journal of Geophysical Research: Space Physics*, 121, 4055–4071. <https://doi.org/10.1002/2015JA021272>
- Thorne, R. M., Armstrong, T. P., Stone, S., Williams, D. J., McEntire, R. W., Bolton, S. J., et al. (1997). Galileo evidence for rapid interchange transport in the Io torus. *Geophysical Research Letters*, 24, 2131–2134. <https://doi.org/10.1029/97GL01788>
- Tsuchiya, F., Kagitani, M., Terada, N., Kasaba, Y., Yoshikawa, I., Murakami, G., et al. (2010). Plan for observing magnetospheres of outer planets by using the EUV spectrograph onboard the SPRINT-A/EXCEED mission. *Advances in Geosciences*, 25, 57–71. https://doi.org/10.1142/9789814355377_0005
- Vasyliūnas, V. M. (1983). Plasma distribution and flow. In A. J. Dessler (Ed.), *Physics of the Jovian Magnetosphere* (pp. 395–453). New York: Cambridge University Press. <https://doi.org/10.1017/CBO9780511564574.013>
- Vogt, M. F., Jackman, C. M., Slavin, J. A., Bunce, E. J., Cowley, S. W. H., Kivelson, M. G., & Khurana, K. K. (2014). Structure and statistical properties of plasmoids in Jupiter's magnetotail. *Journal of Geophysical Research: Space Physics*, 119, 821–843. <https://doi.org/10.1002/2013JA019393>
- Woch, J., Krupp, N., & Lagg, A. (2002). Particle bursts in the Jovian magnetosphere: Evidence for a near-Jupiter neutral line. *Geophysical Research Letters*, 29(7), 1138. <https://doi.org/10.1029/2001GL014080>
- Woch, J., Krupp, N., Lagg, A., Wilken, B., Livi, S., & Williams, D. J. (1998). Quasi-periodic modulations of the Jovian magnetotail. *Geophysical Research Letters*, 25(8), 1253–1256. <https://doi.org/10.1029/98GL00861>
- Wu, H., Hill, T. W., Wolf, R. A., & Spiro, R. W. (2007). Numerical simulation of fine structure in the Io plasma torus produced by the centrifugal interchange instability. *Journal of Geophysical Research*, 112, A02206. <https://doi.org/10.1029/2006JA012032>
- Yang, Y. S., Wolf, R. A., Spiro, R. W., Hill, T. W., & Dessler, A. J. (1994). Numerical simulation of torus-driven plasma transport in the Jovian magnetosphere. *Journal of Geophysical Research*, 99(A5), 8755–8770. <https://doi.org/10.1029/94JA00142>
- Yoneda, M., Kagitani, M., Tsuchiya, F., Sakanoi, T., & Okano, S. (2015). Brightening event seen in observations of Jupiter's extended sodium nebula. *Icarus*, 261, 31–33. <https://doi.org/10.1016/j.icarus.2015.07.037>
- Yoshikawa, I., Suzuki, F., Hikida, R., Yoshioka, K., Murakami, G., Tsuchiya, F., et al. (2017). Volcanic activity on Io and its influence on the dynamics of Jovian magnetosphere observed by EXCEED/Hisaki in 2015. *Earth, Planets and Space*, 69(1), 110. <https://doi.org/10.1186/s40623-017-0700-9>
- Yoshikawa, I., Yoshioka, K., Murakami, G., Suzuki, F., Hikida, R., Yamazaki, A., et al. (2016). Properties of hot electrons in the Jovian inner-magnetosphere deduced from extended observations of the Io plasma torus. *Geophysical Research Letters*, 43, 11,552–11,557. <https://doi.org/10.1002/2016GL070706>
- Yoshioka, K., Murakami, G., Yamazaki, A., Tsuchiya, F., Kimura, T., Kagitani, M., et al. (2014). Evidence for global electron transportation into the Jovian inner magnetosphere. *Science*, 345(6204), 1581–1584. <https://doi.org/10.1126/science.1256259>
- Yoshioka, K., Murakami, G., Yamazaki, A., Tsuchiya, F., Kagitani, M., Sakanoi, T., et al. (2013). The extreme ultraviolet spectroscopy for planetary science, EXCEED. *Planetary and Space Science*, 85, 250–260. <https://doi.org/10.1016/j.pss.2013.06.021>
- Yoshioka, K., Tsuchiya, F., Kimura, T., Kagitani, M., Murakami, G., Yamazaki, A., et al. (2017). Radial variation of sulfur and oxygen ions in the Io plasma torus as deduced from remote observations by Hisaki. *Journal of Geophysical Research: Space Physics*, 122, 2999–3012. <https://doi.org/10.1002/2016JA023691>
- Yoshioka, K., Yoshikawa, I., Tsuchiya, F., Kagitani, M., & Murakami, G. (2011). Hot electron component in the Io plasma torus confirmed through EUV spectral analysis. *Journal of Geophysical Research*, 116, A09204. <https://doi.org/10.1029/2011JA016583>